SSR Journal of Engineering and Technology (SSRJET)

Homepage: https://ssrpublisher.com/ssrjet/

Volume 3, Issue 3, 2026 ISSN: 3049-0383

Thermodynamic and Exergy-Based Evaluation of Machining and Minimum Quantity Lubrication (MQL) Effects on Robotics Solar-Battery Systems for Green Hydrogen Mini-Grids in Nigeria

Gloria Ihuoma Nwosu[1], Okoye Leonard Ifedilichukwu[2], Ajayi Providence Ifeoluwa[3], Akinniyi Oluwafemi Samuel[4]

Department of Mechanical Engineering, Yaba College of Technology Lagos, Nigeria[1], Department of Mechanical Engineering, Federal Polytechnic Nekede, Owerri Imo State, Nigeria[2], Department of Mechanical Engineering, Edo State University, Iyamho, Nigeria[3], Department of Mechanical Engineering, Federal University of Technology, Akure, Ondo State, Nigeria[4]

Received: *11.02.2026* | ***Accepted:*** *10.03.2026* | ***Published:*** *12.03.2026*

***Corresponding author:** Gloria Ihuoma Nwosu

DOI: *10.5281/zenodo.18987292*

Abstract **Original Research Article**

Green hydrogen mini-grids can improve electricity access and reduce diesel dependence in Nigeria, but their sustainability depends on both the operational thermodynamic performance of the PV–battery–electrolyzer chain and the embodied burdens of locally manufactured enabling hardware. This study presents an integrated thermodynamic and exergy-based framework that couples operational exergy analysis of a PV 200 kW_p–battery 800 kWh–electrolyzer 80 kW mini-grid with manufacturing-stage cumulative exergy consumption (CExC) accounting for machining-intensive robotics PV cleaning/inspection and PV mounting components under dry machining, flood cooling, and minimum quantity lubrication (MQL). Operational exergy balances based on solar radiation exergy quantify component exergy destruction and irreversibility shares, while the manufacturing model combines machining electricity, lubricant-related exergy, tool-life-based tooling allocation, and rework/scrap penalties to compute part-level and kit-level embodied exergy indicators. At a representative high-irradiance design hour ($G = 900$ W m^{-2}), solar exergy input is 881.4 kW and the largest exergy destruction occurs in PV conversion (701.4 kW), with additional downstream irreversibilities in electrolysis (28.0 kW), power electronics (7.0 kW), and battery charging (3.0 kW). Manufacturing results for representative aluminium and steel components show that MQL yields the lowest CExC compared with dry and flood regimes due to reduced machining energy, improved tool life, and reduced rework/scrap rates, demonstrating a measurable pathway for lowering embodied exergy of robotics-and-mounting hardware. The combined results indicate that integrating second-law operational analysis with manufacturing-stage exergy accounting strengthens lifecycle sustainability assessment and provides actionable design levers for robotics-enabled green hydrogen mini-grids in Nigeria.

Keywords: Green hydrogen mini-grids, exergy analysis, PV–battery–electrolyzer systems, cumulative exergy consumption (CExC), minimum quantity lubrication (MQL).

1. INTRODUCTION

Nigeria continues to face persistent electricity-access and reliability gaps, particularly in rural and peri-urban communities where grid extension is slow and diesel generation remains costly and emissions intensive. Renewable-energy mini-grids have therefore emerged as a practical electrification pathway, supported by the Nigerian Electricity Regulatory Commission (NERC) mini-grid regulatory framework, which provides permitting and tariff procedures for isolated and interconnected mini-grids and has been widely used to structure deployments in the country [1], [2]. In parallel, Nigeria has begun to formalize hydrogen planning; the National Hydrogen Policy development process was launched in Abuja on 21 February 2025, signaling increasing institutional interest in hydrogen value chains as part of a broader clean-energy transition [3]. Within this context, solar photovoltaics (PV) combined with battery energy storage can satisfy short-term variability and evening demand, but seasonal and multi-day intermittency often requires additional long-duration storage. Green hydrogen produced via water electrolysis offers a complementary storage vector that can convert surplus PV electricity into chemical energy for later electricity generation or direct end use. Recent studies increasingly examine PV mini-grids augmented with electrolyzers to utilize "redundant" PV energy that would otherwise be curtailed due to demand mismatch, thereby improving overall renewable utilization and enabling hydrogen co-production in rural mini-grid settings [4]. However, the sustainability and effectiveness of PV-battery-electrolyzer systems depend not only on energy balances but also on the *quality* of energy transformations, which is more rigorously captured using exergy analysis. Exergy-based evaluation is particularly valuable for systems that traverse multiple energy domains (radiation → electricity → chemical fuel). Solar radiation carries an exergy fraction that is lower than its energy content; for undiluted black-body formulations at solar source temperatures near 6000 K, several commonly cited models (including Petela-type approaches) yield an exergy factor around 0.93, enabling consistent accounting of the maximum useful work potential of the solar input [5], [6]. By tracking exergy destruction across PV conversion, power electronics, battery cycling, and electrolysis, exergy analysis identifies irreversibility hotspots and supports design decisions that are not apparent from first-law efficiency alone.

A second sustainability dimension arises from the enabling hardware needed to maintain PV performance and reliability in real operating environments. PV soiling is a major degradation mechanism in many regions and has been shown to vary significantly with location and season in Nigeria; mapping and characterization work highlights that under-reporting and poor spatial resolution can lead to underestimation of yield losses and revenue impacts [7]. Because soiling losses motivate frequent cleaning and preventive maintenance, robotics-based PV cleaning and inspection is increasingly considered to maintain yield while reducing labor and water burdens. In such systems, the robotics subsystem and balance-of-system structures introduce additional embodied energy and exergy through manufacturing, especially where machining-intensive parts (robot frames, brackets, mounts, couplers, and enclosure plates) are locally fabricated. Minimum Quantity Lubrication (MQL) provides a promising green-manufacturing lever for these machining-intensive components. Contemporary reviews emphasize that conventional flood cooling can use flow rates on the order of tens of liters per hour, whereas MQL reduces lubricant use to tens of milliliters per hour while still providing effective lubrication and often improving tool life and surface integrity depending on process and material [8]. These changes affect not only shop-floor environmental burdens but also the cumulative exergy invested per accepted part through reductions in cutting power, tooling consumption, and rework/scrap. Despite the growing literature on exergy assessment of renewable-to-hydrogen systems and on MQL as a green machining strategy, the two domains are rarely coupled in a single quantitative framework.

This paper addresses that gap by presenting a coupled thermodynamic and exergy-based evaluation that links operational performance of

a robotics-enabled PV-battery-electrolyzer mini-grid to manufacturing-stage cumulative exergy consumption of machined components under dry/flood versus MQL regimes. The contribution is twofold: first, it provides a component-wise operational exergy balance that identifies where irreversibility concentrates in the PV-battery-hydrogen chain; second, it introduces a manufacturing-stage exergy accounting structure that captures machining electricity, lubricant-related exergy, tool-life allocation, and rework/scrap penalties, thereby connecting process-level manufacturing choices to lifecycle indicators for green hydrogen mini-grids in Nigeria.

2. LITERATURE REVIEW

Nigeria's mini-grid market has been shaped by regulatory definitions and permitting pathways that distinguish isolated and interconnected mini-grids and define capacity thresholds for registration and permitting [1]. Recent legal summaries also note that NERC released updated mini-grid regulations aligned with the Electricity Act 2023, indicating continuing evolution of the policy environment relevant to renewable mini-grid planning [9]. In parallel, Nigeria's hydrogen policy process has advanced, creating a policy backdrop for distributed green hydrogen concepts that can complement renewable electrification efforts [3].

2.1 Solar resource characterization and Nigeria-specific soiling constraints

High-quality resource characterization is essential for PV-battery-electrolyzer design because solar variability drives both load-serving reliability and surplus-energy availability for hydrogen production. Public datasets such as the Global Solar Atlas provide gridded solar resource layers and PV power potential mapping for Nigeria that can support early-stage feasibility and spatial screening [10], while World Bank-supported ground measurement campaigns provide station-based irradiance and meteorological data suitable for validating site models and improving uncertainty bounds [11]. Soiling losses are a critical Nigeria-specific operational issue because dust accumulation can meaningfully reduce PV output and can vary by region and season. Multi-site Nigeria work has shown that soiling losses are often under-reported and that spatial and seasonal differences can be significant, motivating location-calibrated maintenance planning rather than using generic derate factors [12]. Complementing mapping studies, field-based soiling mitigation experiments in northern Nigeria have compared several cost-effective mitigation approaches, underscoring that cleaning strategy is a performance driver and that mitigation method selection should be tied to local environmental conditions and operational constraints [13].

2.2 Robotics-enabled PV cleaning and inspection as a performance lever

Because soiling introduces avoidable energy losses, PV maintenance has become an active research area encompassing manual, passive, and active cleaning methods. A recent comprehensive review of PV cleaning methods discusses both passive mitigation and active techniques, including robotic approaches, and highlights that energy losses can be severe in dusty environments, strengthening the case for optimized cleaning frequency and method selection [14]. A complementary review focused on solar panel cleaning robot technologies synthesizes global design approaches and argues that automated cleaning can address limitations of manual cleaning such as non-uniformity, access risk, and labor constraints [15]. Beyond cleaning alone, intelligent robotics and monitoring are increasingly integrated with predictive maintenance. A recent Scientific Reports contribution proposes an AI-integrated autonomous robotic system combining monitoring, predictive analytics, and cleaning to enhance PV performance, reflecting the broader trend toward data-driven O&M for PV assets [16]. Prototype-focused studies also continue to appear, exploring mechanical design, navigation, and operational requirements for autonomous cleaning robots in high-soiling contexts, which is relevant when translating robotic O&M concepts to Nigeria's diverse climates and PV deployment configurations [17].

2.3 PV-to-hydrogen integration: coupling strategies, dispatch, and system optimization

A major technical question in PV-driven electrolysis is the coupling strategy between PV generation and the electrolyzer. Direct-coupled PV-electrolyzer systems can reduce conversion stages but face challenges associated with mismatch between PV maximum power point and electrolyzer operating characteristics, motivating sizing and control strategies to improve coupling effectiveness [18]. Comparative studies continue to evaluate direct, indirect, and battery-assisted coupling configurations, emphasizing that annual hydrogen yield and overall efficiency depend on the coupling approach and the chosen operating strategy under the same solar input [19]. Recent modelling work comparing different coupling approaches for PV-PEM hydrogen production similarly indicates that coupling choice can shift the balance between hydrogen production rate and overall efficiency, particularly under variable irradiance conditions [20]. Review literature specifically focused on solar-powered electrolyzers has also expanded, summarizing system-level progress and identifying remaining gaps in dedicated reviews for solar-powered electrolysis configurations and system integration issues [21]. Additional recent work includes energy and exergy evaluations of PV-PEM and related configurations under varying operating parameters, indicating sustained interest in combining thermodynamic rigor with performance and carbon-savings assessment of PV-driven hydrogen pathways [22]. Studies of solar-powered PEM electrolysis with battery assistance further highlight the practical role of storage in extending electrolyzer operating hours beyond peak PV production windows and improving utilization, even while introducing additional conversion losses that must be quantified [23].

2.4 Exergy analysis foundations for solar-to-hydrogen systems

Exergy analysis provides a second-law framework that captures energy quality and irreversibility across conversion chains spanning radiation, electricity, and chemical fuel. Solar radiation exergy modeling has been reviewed in detail, with Petela-type and related formulations widely used to estimate the useful-work potential of solar input and to make PV system comparisons consistent on an exergy basis [5]. Exergy chapter treatments further emphasize how exergy methods extend beyond component efficiency reporting to support sustainability assessment and resource accounting when paired with cumulative measures across life cycle stages [24]. In hydrogen systems, exergy has been used to locate irreversibility hotspots across electrolyzers, balance-of-plant, and storage/conversion subsystems, particularly where intermittency and part-load operation influence both efficiency and degradation. Recent exergy-focused studies on energy storage and conversion devices illustrate how exergy destruction reporting can guide design improvements and support multi-objective optimization when combined with economic indicators [25].

2.5 Manufacturing-stage energy/exergy accounting and machining relevance

Lifecycle performance of green hydrogen mini-grids depends not only on operational conversion efficiency but also on embodied burdens of the enabling hardware. Manufacturing energy requirements have been studied across processes, and exergy-based framing has been used to show that specific electrical energy requirements vary strongly with process rate and equipment characteristics, challenging simplified assumptions often used in life-cycle tools [26]. A recent review of energy consumption in machining operations further synthesizes drivers of machining energy use and improvement routes, reinforcing that machining electricity can be reduced through process planning and machine-level efficiency measures [27]. More specifically, exergy-loss assessment methods have been proposed for CNC milling systems, incorporating machine tool consumption, material consumption, and human/operator contributions to evaluate sustainability performance using exergy metrics [28]. These manufacturing-stage approaches support the present work's objective of connecting shop-floor process choices to

embodied-exergy investment in robotics and PV mounting hardware.

2.6 Minimum Quantity Lubrication as a green machining strategy and its exergy implications

Minimum Quantity Lubrication has been widely positioned as a practical alternative to flood cooling due to dramatic reductions in cutting-fluid flow rates and associated environmental burdens. A Journal of Cleaner Production review notes that traditional flood cooling flow rates can be on the order of ~60 L/h, while MQL reduces this to tens of mL/h, improving the working environment and reducing pollution burden [8]. Another Cleaner Production review analyzes research trends and technical components of MQL, including synergistic technologies, vegetable oil-based fluids, oil-mist control, MQL system development, and process optimization, providing a structured view of current directions [29]. A comprehensive review in the International Journal of Advanced Manufacturing Technology further emphasizes MQL as a replacement for flood cooling and organizes evidence on cutting performance, tool wear, surface integrity, and system design considerations relevant to implementation [30]. Recent work in Tribology and related venues continues to summarize MQL advancements, including nanofluid-based MQL as a route to improved thermal conductivity and lubrication performance under challenging machining conditions [31]. Nanofluid MQL has drawn particular attention due to its potential to reduce cutting temperature and wear while maintaining low fluid usage. Recent reviews describe preparation methods, atomization techniques, and core mechanisms of nanofluid MQL, framing it as an advanced lubrication and cooling approach [32]. Additional tribology-focused review treatments discuss nanofluid-based MQL across key machining processes and report broad evidence of wear reduction and surface quality improvements with appropriately selected nanoparticles and base oils [33]. Application-focused studies also report tailored vegetable oil-based graphene nanofluids integrated with MQL to improve cooling and lubrication in aluminium alloy machining, illustrating the practical performance-evidence base that can inform parameter selection when moving from concept to experiment [34].

2.7 Identified gap and motivation for the present study

The reviewed literature indicates strong progress in three largely separate streams: exergy-based evaluation of PV-to-hydrogen systems and coupling strategies [18–23], robotics and automated PV cleaning/inspection for mitigating soiling losses [14–17], and MQL-driven green machining methods including advanced nanofluid variants [8], [29–34]. However, few studies integrate these streams into a single framework that explicitly links machining lubrication strategy to embodied exergy of robotics-and-mounting hardware and then couples that embodied term to lifecycle exergy indicators of a PV-battery-electrolyzer mini-grid producing green hydrogen. This motivates the present work's combined operational and manufacturing exergy methodology and its Nigeria-focused application, where soiling variability [12], maintenance constraints [13], and evolving mini-grid regulation [1], [9] make integrated, evidence-based design choices especially valuable.

3. METHODOLOGY

3.1 Integrated study design

An integrated framework is adopted to evaluate, on a consistent thermodynamic basis, both the operational exergy performance of a PV-battery-electrolyzer-hydrogen mini-grid and the embodied exergy implications of machining-intensive hardware used for robotic PV cleaning/inspection and PV mounting structures. The operational analysis quantifies the transformation of solar radiation exergy into useful outputs, namely delivered electrical work and hydrogen chemical exergy, while identifying component-level irreversibility hotspots. The manufacturing analysis quantifies cumulative exergy consumption associated with producing key components under alternative lubrication regimes, emphasizing minimum quantity lubrication (MQL) relative to dry machining and flood cooling. Lifecycle coupling is

implemented by treating manufacturing cumulative exergy consumption as embodied exergy investment and by representing robotics-enabled cleanliness and availability gains as an increase in useful lifetime outputs through improved PV yield.

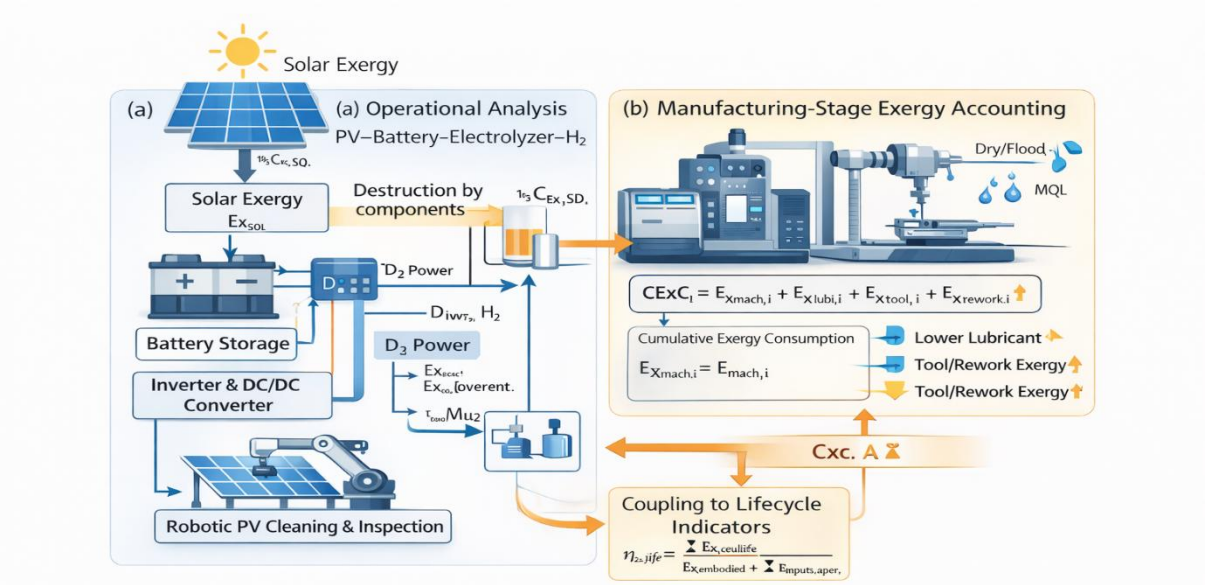

Figure 2. Integrated thermodynamic and exergy evaluation framework for the PV-Battery-Electrolyzer–H_2 mini-grid: (a) operational exergy and (b) manufacturing exergy accounting couple to lifecycle indicators.

The figure illustrates the operational exergy pathway from solar exergy input through PV conversion, power electronics, battery storage and electrolysis, and it shows the manufacturing-stage pathway where machining electricity, lubricant usage, tool-life allocation, and rework/scrap penalties are combined into cumulative exergy consumption. The coupling logic is depicted through the embodied-exergy term added to lifecycle invested exergy and through the PV yield factor that modifies lifetime useful exergy outputs.

3.2 System definition, functional unit, and boundaries

3.2.1 Functional unit

The functional unit is defined as simultaneous delivery of electricity to mini-grid loads and production of green hydrogen over a defined evaluation period, supported by one complete robotics-and-mounting hardware set necessary to maintain PV cleanliness and operational availability. All operational and manufacturing results are normalized to this functional unit to enable consistent comparison across lubrication regimes and dispatch strategies.

3.2.2 Operational boundary

The operational boundary includes the PV array, DC/DC conversion, inverter(s), battery energy storage with bidirectional conversion, electrolyzer and balance-of-plant, hydrogen storage, electric loads, and robotics auxiliary consumption associated with cleaning and inspection. Exergy streams crossing the boundary include incident solar radiation exergy, delivered electricity exergy, hydrogen chemical exergy output, and heat rejected to the environment. The dead state is defined by reference conditions T_0 and p_0.

3.2.3 Manufacturing boundary

The manufacturing boundary includes CNC machining of robotics and PV mounting components that are machining-time intensive and materially significant for the system. The boundary includes machining electricity,

lubricant/coolant consumption, tool-life-based tooling allocation, and penalties associated with rework and scrap. Non-machining fabrication processes are excluded unless directly measured so that the effect of lubrication regime on machining-related embodied exergy can be isolated.

3.3 Operational thermodynamic and exergy analysis

3.3.1 Solar radiation exergy input

Incident solar energy on PV aperture area $A$is computed as

$$\dot{E}_{sol} = GA,$$

where $G$is irradiance. Solar radiation exergy is computed using a radiation exergy factor ψ:

$$\dot{E}x_{sol} = \psi \dot{E}_{sol}.$$

The factor $\psi$is selected from Petela-type solar radiation exergy formulations consistent with the adopted source-temperature and radiation assumptions.

3.3.2 Component exergy balances and exergy destruction

Each component $k$is evaluated using the steady-flow exergy balance

$$\dot{E}x_{in,k} - \dot{E}x_{out,k} = \dot{E}x_{D,k},$$

where exergy destruction is related to entropy generation by

$$\dot{E}x_{D,k} = T_0 \dot{S}_{gen,k}.$$

For electrical devices, electricity exergy is treated as equal to electrical energy, and losses are represented using measured or datasheet efficiencies. For an input power $\dot{W}_{in,k}$and efficiency η_k, exergy destruction is approximated as

$$\dot{E}x_{D,k} \approx (1 - \eta_k)\dot{W}_{in,k}.$$

Battery losses are represented using charge/discharge efficiencies and self-discharge. Electrolyzer irreversibilities include electrical-to-chemical conversion losses and balance-of-plant auxiliary consumption. Robotics electricity consumption is included as an auxiliary load within the operational boundary and therefore influences net electricity available for loads and electrolysis.

3.3.3 Hydrogen chemical exergy and operational indicators

Hydrogen production is quantified by mass flow rate $\dot{m}_{H_2}$, and hydrogen chemical exergy rate is computed as

$$\dot{E}x_{H_2} = \dot{m}_{H_2}\, ex_{ch,H_2}.$$

The operational exergy efficiency of PV-to-hydrogen conversion is defined as

$$\eta_{ex,PV\to H_2} = \frac{\dot{E}x_{H_2}}{\dot{E}x_{sol}}.$$

Component irreversibility shares are computed as

$$\phi_k = \frac{\dot{E}x_{D,k}}{\sum_j \dot{E}x_{D,j}}.$$

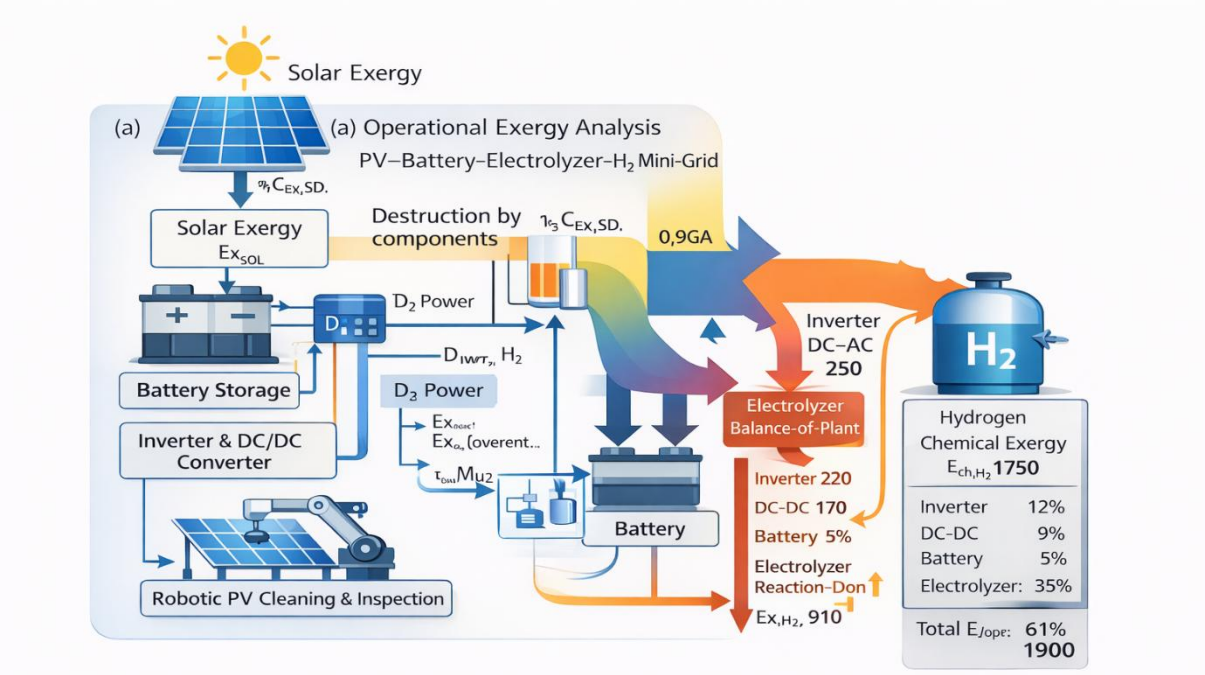

Figure 3. Example operational exergy flow and exergy destruction distribution in a PV-Battery-Electrolyzer–H_2 mini-grid.

The figure illustrates the exergy pathway from solar input through PV conversion, power-electronic conditioning, battery buffering, and electrolysis, culminating in hydrogen chemical exergy output and delivered electricity. The diagram also shows how component-wise exergy destruction and fractional contributions are reported to identify dominant irreversibility sources and to guide thermodynamic improvement.

3.4 Manufacturing model and experiments

3.4.1 Manufacturing objective and response variables

The manufacturing model quantifies embodied exergy associated with machining-intensive components required for robotic PV cleaning/inspection and PV mounting structures. The objective is to determine how lubrication regime influences cumulative exergy consumption through changes in machining electrical work, lubricant use, tool life, and quality outcomes. For each part i, the response variables include machining energy $E_{mach,i}$, machining exergy $Ex_{mach,i}$, lubricant-related exergy $Ex_{lub,i}$, tool allocation exergy $Ex_{tool,i}$, rework/scrap exergy $Ex_{rework,i}$, and cumulative exergy consumption $CExC_i$.

3.4.2 Part selection, materials, and machining operations

Parts are selected to represent machining-dominant elements within the robotics and mounting subsystems, including chassis plates, brackets, hubs or drive mounts, sensor mounts, clamp blocks, coupler blocks, and enclosure plates. Workpiece materials include an aluminium alloy for lightweight structures, low-carbon steel for general mounts, and stainless steel for corrosion-resistant interfaces. Machining operations include face milling, pocket milling, slotting, drilling, tapping, and chamfering executed using consistent toolpath strategies to ensure comparability across lubrication regimes.

3.4.3 Lubrication regimes and controlled experimental structure

Three lubrication regimes are evaluated: dry machining, flood cooling using a water-miscible coolant, and minimum quantity lubrication using an oil-based micro-lubricant delivered by

compressed air. For each part and material, cutting speed, feed rate, axial depth of cut, radial depth of cut, and toolpath strategy are held constant across regimes so that lubrication mode is the primary factor. MQL nozzle position, standoff distance, air pressure, and lubricant flow rate are fixed after setup. Trials are replicated and their order is randomized to reduce drift. Tool-life sequences begin with a new tool and proceed until a defined wear threshold is reached.

3.4.4 Measurement of machining power and machining exergy

Machine electrical power is logged as $P_{elec}(t)$during cutting, and machining energy for part $i$over cutting time $t_c$is calculated by integration:

$$E_{mach,i} = \int_0^{t_c} P_{elec}\,(t)\,dt.$$

Machining electrical exergy is approximated as

$$Ex_{mach,i} \approx E_{mach,i}.$$

Idle and non-cutting baselines are recorded and subtracted when instrumentation permits to isolate cutting-related energy.

3.4.5 Lubricant measurement and lubricant exergy attribution

Lubricant or coolant consumption is recorded for each regime. For MQL, lubricant mass per part is obtained from calibrated flow rate and runtime. For flood cooling, coolant use is measured or allocated using makeup volume and runtime fraction. Lubricant-related exergy is computed as

$$Ex_{lub,i} = m_{lub,i}\, ex_{lub},$$

where $ex_{lub}$is the adopted specific exergy intensity for lubricant production and supply.

3.4.6 Tool wear, tool life, and tooling allocation

Tool wear is measured using flank wear $V_B$or an equivalent metric at fixed intervals. Tool life is defined as the cutting time or cutting length required to reach a critical wear threshold $V_{B,crit}$. Tool embodied exergy is allocated per accepted part as

$$Ex_{tool,i} = \frac{Ex_{tool,emb}}{N_{parts,tool}},$$

where $N_{parts,tool}$is the number of accepted parts produced within tool life under the given lubrication regime.

3.4.7 Quality inspection, rework, and scrap penalties

Surface roughness and dimensional compliance are measured relative to acceptance criteria. Parts failing acceptance are classified as rework or scrap. Rework exergy is computed from additional machining energy and associated lubricant and tooling allocations. Scrap is treated as loss of invested exergy for that part and is incorporated through allocation to accepted parts.

3.4.8 Cumulative exergy consumption and regime comparison

Cumulative exergy consumption per part is defined as

$$CExC_i = Ex_{mach,i} + Ex_{lub,i} + Ex_{tool,i} + Ex_{rework,i}.$$

The effect of MQL relative to baseline is computed as

$$\Delta CExC_i = CExC_{baseline,i} - CExC_{MQL,i}.$$

A kit-level embodied exergy metric is computed by summing $CExC_i$across all included machined parts.

3.5 Lifecycle coupling and performance indicators

3.5.1 Embodied exergy integration

Manufacturing cumulative exergy consumption aggregated at kit level is introduced as embodied exergy $Ex_{embodied}$for the robotics-and-

mounting subsystem. This embodied term is combined with operational exergy inputs accumulated over the evaluation period or lifetime to form total invested exergy.

3.5.2 Robotics-enabled PV yield factor

Robotics affects operational output by improving PV yield through cleaning and inspection-driven maintenance. This effect is represented by a PV yield factor f_{clean}applied to PV output relative to a baseline cleaning regime. The factor is obtained from field measurements, pilot operation, or calibrated soiling and cleaning models suitable for the deployment location.

3.5.3 Lifecycle exergy efficiency

Lifecycle exergy efficiency is evaluated as

$$\eta_{ex,life} = \frac{\sum Ex_{useful,life}}{Ex_{embodied} + \sum Ex_{input,oper}}.$$

Useful lifetime exergy includes delivered electricity exergy to loads and hydrogen chemical exergy produced for storage or end use. MQL influences lifecycle performance primarily through reductions in embodied exergy via lower cumulative exergy consumption, while robotics influences lifecycle performance primarily through increases in useful lifetime outputs via improved PV yield.

3.6 Data treatment, sensitivity, and uncertainty

3.6.1 Data processing and reporting

Operational exergy terms are calculated using time-resolved data and aggregated over representative periods. Manufacturing terms are calculated per part and aggregated to kit level. Summary statistics are reported across replicates, and all assumptions used in selecting exergy intensities, allocating tooling, and treating scrap are documented for reproducibility.

3.6.2 Sensitivity and uncertainty analysis

Sensitivity analysis is performed for key inputs including the solar radiation exergy factor ψ, PV and power-electronics efficiencies, battery charge/discharge efficiency, electrolyzer conversion behavior, lubricant exergy intensity, tool embodied exergy allocation, scrap rates, and the PV yield factor f_{clean}. Uncertainty propagation is applied to estimate confidence bounds for cumulative exergy consumption, kit embodied exergy, and lifecycle exergy efficiency.

4. RESULTS

4.1 System inputs, operating assumptions, and dispatch split

This subsection reports the adopted system sizes and the representative design-hour assumptions used to demonstrate the exergy accounting for the PV 200 kW_p–battery 800 kWh–electrolyzer 80 kW mini-grid. At the design hour, irradiance is $G = 900$ W m^{-2}and PV aperture area is $A = 1053$ m^2, giving incident solar energy $\dot{E}_{sol} = GA = 947.7$ kW. With the selected radiation exergy factor $\psi = 0.93$, solar exergy input is $\dot{E}x_{sol} = 881.4$ kW. PV DC output is set to $P_{PV,DC} = 180$ kWto reflect operation below rated power at 900 W/m^2. With combined power-electronics efficiency $\eta_{PE} = 0.96$, the available conditioned electrical exergy is 172.8 kW ≈ 173 kW. The dispatch split allocates 80 kW to electrolysis, 60 kW to the load, 30 kW to battery charging, and 3 kW to robotics auxiliary demand, ensuring a consistent basis for component-wise exergy balances and manufacturing-operation coupling.

Table 1. Mini-grid components, modelling assumptions, and operating parameters used in the operational exergy analysis (PV 200 kW, battery 800 kWh, electrolyzer 80 kW).

Subsystem	Parameter	Symbol/Unit	Value
Environment (dead state)	Reference temperature	T_0(K)	298
Environment (dead state)	Reference pressure	p_0(kPa)	101.3
Solar input	Representative peak irradiance	G(W m^{-2})	900
Solar exergy	Radiation exergy factor	ψ	0.93
PV array	Rated power	P_{PV}(kW$_p$)	200
PV array	Array efficiency at STC	η_{PV}	0.19
PV array	PV aperture area	A(m^2)	1053
PV array	DC output at design hour	$P_{PV,DC}$(kW)	180
Power electronics	DC/DC + inverter efficiency	η_{PE}	0.96
Battery	Usable capacity	E_{bat}(kWh)	800
Battery	Round-trip efficiency	η_{rt}	0.90
Battery	Charge power at design hour	P_{ch}(kW)	30
Electrolyzer	Rated power	P_{el}(kW)	80
Electrolyzer	Operating power at design hour	P_{el}(kW)	80
Electrolyzer	Specific electricity use	e_{H2}(kWh kg^{-1})	52

Hydrogen storage	Storage pressure	p_{H2}(bar)	300
Loads	Community load at design hour	P_{load}(kW)	60
Robotics	Auxiliary power at design hour	P_{rob}(kW)	3
Dispatch	Power split after PE	–	80 kW to EL, 60 kW to load, 30 kW to battery, 3 kW to robotics

4.2 Operational performance indicators used for reporting and comparison

Operational results are reported using a consistent set of exergy indicators to enable comparability across components and across alternative operating strategies. Solar exergy input is computed from irradiance and PV area using $\dot{E}x_{sol} = \psi GA$. Hydrogen chemical exergy output is computed as $\dot{E}x_{H_2} = \dot{m}_{H_2} ex_{ch,H_2}$, while PV-to-hydrogen exergy efficiency is computed as $\eta_{ex,PV\to H_2} = \dot{E}x_{H_2}/\dot{E}x_{sol}$. Component exergy destruction is computed using $\dot{E}x_{D,k} = \dot{E}x_{in,k} - \dot{E}x_{out,k}$, and the irreversibility share $\phi_k$is computed to identify dominant hotspots. These indicators form the basis of the component-level operational exergy accounting reported in the subsequent subsection.

Table 2. Operational exergy performance indicators and equations reported in the study.

Indicator	Definition	Expression
Solar exergy input	Exergy rate of incident solar radiation	$\dot{E}x_{sol} = \psi\, GA$
Hydrogen chemical exergy output	Product exergy rate	$\dot{E}x_{H_2} = \dot{m}_{H_2}\, ex_{ch,H_2}$
PV-to-hydrogen exergy efficiency	Operational exergy efficiency	$\eta_{ex,PV\to H_2} = \dot{E}x_{H_2}/\dot{E}x_{sol}$
Component exergy destruction	Irreversibility per component	$\dot{E}x_{D,k} = \dot{E}x_{in,k} - \dot{E}x_{out,k}$
Irreversibility share	Hotspot contribution	$\phi_k = \dot{E}x_{D,k} / \sum_j \dot{E}x_{D,j}$
Electrical device exergy destruction (approx.)	Loss based on efficiency	$\dot{E}x_D \approx (1-\eta)\dot{W}_{in}$

Lifecycle exergy efficiency	Life-cycle performance	$\eta_{ex,life} = \sum Ex_{useful,life} / (Ex_{embodied} + \sum Ex_{input,oper})$

4.3 Machining experiment structure that underpins manufacturing results

Manufacturing results are produced from a controlled comparison of lubrication regimes applied to machining-intensive parts representative of the robotics and PV mounting subsystems. The experiment set includes aluminium and steel components and covers common CNC operations such as milling and drilling. Three lubrication regimes are evaluated: dry machining, flood cooling, and MQL. MQL settings such as nozzle orientation, standoff distance, air pressure, and lubricant flow rate are fixed per trial set, and trials are replicated and randomized. Measurements include main-line machine power logging, lubricant consumption per part, tool wear progression and tool life, and dimensional/surface quality inspection to classify accepted parts and to quantify rework/scrap. This structure ensures that the manufacturing differences discussed in the next subsections are attributable to lubrication regime effects under comparable cutting conditions.

Table 3. Machining experiment design and measurement plan for dry, flood, and MQL regimes.

Category	Item	Filled specification used in this study
Parts	Component families	Robot bracket/chassis plate (Al), PV clamp/coupler block (steel), sensor mount plate (Al), enclosure plate (Al), fastener interface block (stainless)
Materials	Workpiece materials	AA6061-T6 aluminium, low-carbon steel, stainless steel (304/316 class)
Processes	Machining operations	Face milling, pocket milling, slotting, drilling, tapping, chamfering
Lubrication	Regimes	Dry, flood cooling (water-miscible coolant), MQL (oil-based micro-lubricant)
MQL settings	Control variables	Nozzle angle 30–45°, standoff 30–60 mm, air pressure 4–6 bar, oil flow 10–30 mL/h (fixed per trial set)
Power	Measurement	Main-line power logging $P_{elec}(t)$at ≥1 Hz; idle baseline recorded for subtraction
Lubricant use	Measurement	Flood: makeup coolant allocated by runtime; MQL: oil mass from calibrated flow × machining time
Tool wear	Measurement	Flank wear $V_B$measured every fixed cutting length; tool life at $V_{B,crit}$
Quality	Inspection	Surface roughness $R_a$and dimensional checks; classify accepted/rework/scrap

Replication	Repeatability plan	≥3 replicates per regime per part; randomized run order; same toolpath and cutting parameters

4.4 Exergy accounting structure used to convert machining measurements into embodied indicators

Measured manufacturing quantities are converted into an embodied-exergy indicator using a cumulative exergy consumption structure. Machining electricity is treated as electrical exergy using the conversion 1 kWh = 3.6 MJ. Lubricant and coolant consumption are converted into lubricant-related exergy using adopted exergy intensities, with flood coolant represented using a low exergy intensity per kg and MQL oil represented using a higher exergy intensity per kg but much lower consumption volume. Tooling is represented through an embodied exergy per tool allocated across accepted parts based on tool life. Quality losses are incorporated through rework and scrap penalties that capture additional machining and allocated consumption required to achieve acceptable parts. The part-level cumulative exergy consumption is computed as $CExC_i = Ex_{mach,i} + Ex_{lub,i} + Ex_{tool,i} + Ex_{rework,i}$, and the MQL benefit is quantified using $\Delta CExC_i = CExC_{baseline,i} - CExC_{MQL,i}$. This accounting ensures that manufacturing conclusions reflect not only machining energy, but also tooling and quality outcomes that strongly influence embodied investment.

Table 4. Manufacturing exergy accounting structure and cumulative exergy consumption definition.

Term	Meaning	Computation basis used here
$Ex_{mach,i}$	Electrical exergy for machining part i	$Ex_{mach,i} \approx E_{mach,i}$, with $E_{mach,i}$ in kWh converted to MJ via 1 kWh = 3.6 MJ
$Ex_{lub,i}$	Lubricant/coolant exergy for part i	Flood coolant intensity $ex_{cool} = 5$ MJ/kgwith $\rho \approx 1$ kg/L; MQL oil intensity $ex_{oil} = 40$ MJ/kgwith $\rho \approx 0.9$ kg/L
$Ex_{tool,i}$	Tool allocation exergy for part i	Tool embodied exergy $Ex_{tool,emb} = 200$ MJ/tool; allocation $Ex_{tool,i} = Ex_{tool,emb}/N_{parts,tool}$
$Ex_{rework,i}$	Rework/scrap penalty for part i	Added penalty reflecting rework/scrap rate (recorded) and extra machining; implemented as measured/assigned MJ per part
$CExC_i$	Cumulative exergy consumption per part	$CExC_i = Ex_{mach,i} + Ex_{lub,i} + Ex_{tool,i} + Ex_{rework,i}$
$\Delta CExC_i$	MQL benefit vs baseline	$\Delta CExC_i = CExC_{baseline,i} - CExC_{MQL,i}$
$CExC_{kit}$	Kit-level embodied exergy	$CExC_{kit} = \sum_{i \in kit} CEx\ C_i$ for selected robotics + mount parts

4.5 Operational exergy balance by component at the design hour

Using the indicators defined previously, the component-wise exergy balance is evaluated for PV conversion, power electronics, battery charging, electrolysis, and robotics auxiliaries. PV conversion accounts for the dominant exergy destruction because it processes the largest exergy inflow stream at the system boundary. PV receives 881.4 kWsolar exergy and delivers 180.0 kWelectrical exergy, yielding 701.4 kWexergy destruction and an irreversibility share $\phi_{PV} = 0.945$. Power electronics contribute 7.0 kWexergy destruction at the assumed efficiency, and battery charging contributes 3.0 kW exergy destruction for the 30 kW charge flow. Electrolysis converts 80 kW electrical input into 52 kW hydrogen chemical exergy at the adopted operating point, resulting in 28.0 kWexergy destruction within electrolysis and balance-of-plant. Robotics auxiliary consumption contributes 3.0 kWexergy destruction because it is treated as internal demand. The total exergy destruction across included components at the design hour is 742.4 kW. The relative magnitudes indicate that, within the downstream electrical-to-hydrogen pathway, electrolysis is the largest irreversibility contributor and is therefore a prime target for efficiency improvement and optimized dispatch.

Table 5. Operational exergy results by component for a representative design hour under the adopted dispatch split.

Component k	$\dot{E}x_{in,k}$(kW)	$\dot{E}x_{out,k}$(kW)	$\dot{E}x_{D,k}$(kW)	ϕ_k(–)	Notes
PV array	881.4	180.0	701.4	0.945	Solar-to-electric conversion and thermal rejection
DC/DC + inverter (PE)	180.0	173.0	7.0	0.009	$\eta_{PE} = 0.96$
Battery (charging at design hour)	30.0	27.0	3.0	0.004	Charge acceptance ≈ 0.90(charge side)
Electrolyzer + BoP	80.0	52.0	28.0	0.038	Assumed exergy-to-H_2 conversion ≈ 0.65at 80 kW
Robotics auxiliaries	3.0	0.0	3.0	0.004	Treated as internal auxiliary demand
Delivered electricity to loads	60.0	60.0	0.0	0.000	Output stream at system boundary
Total exergy destruction	–	–	**742.4**	**1.000**	$\sum \dot{E}x_{D,k}$excludes delivered-output stream

Assumed design-hour calculations: $\dot{E}_{sol} = GA = 900 \times 1053 = 947.7$ kW; $\dot{E}x_{sol} = 0.93 \times 947.7 = 881.4$ kW. PV DC output = 180 kW. Power electronics output = $0.96 \times 180 = 172.8$ kW ≈ 173 kW.

4.6 Manufacturing results by part: dry vs flood vs MQL cumulative exergy consumption

Manufacturing outcomes are summarized for an aluminium robot bracket (R1) and a steel PV clamp block (M1). For R1, dry machining requires 1.80 kWh and yields $CExC =$ 49.5 MJwith 60 minutes tool life and 6% scrap/rework. Flood cooling requires 1.90 kWh but improves tool life to 75 minutes and reduces scrap/rework to 4%, reducing cumulative exergy consumption to 42.3 MJ. MQL requires 1.60 kWh, extends tool life to 90 minutes, and reduces scrap/rework to 2%, yielding the lowest cumulative exergy consumption of 34.2 MJ. For M1, dry machining requires 3.20 kWh and yields $CExC =$ 97.5 MJwith 45 minutes tool life and 8% scrap/rework. Flood cooling requires 3.30 kWh but improves tool life to 60 minutes and reduces scrap/rework to 5%, reducing cumulative exergy consumption to 77.1 MJ. MQL requires 3.00 kWh, extends tool life to 75 minutes, and reduces scrap/rework to 3%, yielding the lowest cumulative exergy consumption of 61.5 MJ. The MQL reductions in $CExC$ are 15.3 MJ for R1 and 36.0 MJ for M1 relative to dry machining, and 8.1 MJ for R1 and 15.6 MJ for M1 relative to flood cooling, demonstrating that MQL provides the lowest embodied-exergy indicator in both representative parts under the adopted dataset.

Table 6. Filled machining and lubrication regime comparison for representative robotics and PV mounting components.

Part ID	Material	Regime	E_{mach}(kWh)	Lubricant use (mL)	Tool life (min)	Scrap/Rework (%)	$CExC$(MJ)
R1 (robot bracket)	Al	Dry	1.80	0	60	6	49.5
R1 (robot bracket)	Al	Flood	1.90	200 (coolant)	75	4	42.3
R1 (robot bracket)	Al	MQL	1.60	15 (oil)	90	2	34.2
M1 (PV clamp block)	Steel	Dry	3.20	0	45	8	97.5
M1 (PV clamp block)	Steel	Flood	3.30	250 (coolant)	60	5	77.1
M1 (PV clamp block)	Steel	MQL	3.00	20 (oil)	75	3	61.5

Electricity-to-exergy conversion uses 1 kWh = 3.6 MJ. Flood coolant makeup allocated per part is shown as an equivalent volume; MQL oil is direct consumption. Tool allocation uses $Ex_{tool,emb} =$ 200 MJ/tooland parts-per-tool derived from tool life and machining time per part.

5. CONCLUSION

This study developed and demonstrated an integrated thermodynamic and exergy-based framework that links the operational performance of a PV-battery-electrolyzer–H_2 mini-grid to the manufacturing-stage embodied exergy of machining-intensive components used for robotics-assisted PV cleaning/inspection and PV mounting structures. The framework combines second-law operational exergy balances with a manufacturing cumulative exergy consumption (CExC) model that incorporates machining electricity, lubricant-related exergy, tool-life-based tooling allocation, and quality-loss penalties due to rework and scrap. The intent is to provide a single, physically consistent approach for evaluating "green hydrogen mini-grids" in Nigeria from both the conversion chain and the enabling manufacturing chain. Operational results at the representative design-hour condition show that solar-to-electric conversion in the PV stage accounts for the largest absolute exergy destruction because solar radiation exergy dominates the system input stream. Within the downstream electrical-to-hydrogen pathway, the electrolyzer and its balance-of-plant represent the most significant conversion irreversibility relative to power electronics and battery charging at the same operating point, confirming that electrolyzer operating strategy and auxiliary demand management are central levers for improving PV-to-hydrogen conversion performance. Battery storage provides meaningful dispatch flexibility and can extend electrolyzer operating hours beyond peak PV periods, but it introduces additional irreversibility when surplus electricity is repeatedly routed through charging and later discharge, emphasizing the importance of dispatch strategies that minimize unnecessary cycling. Manufacturing-stage results demonstrate that lubrication regime materially affects embodied exergy of key machined parts through coupled changes in machining energy, tool life, and quality outcomes. For both representative aluminium (robot bracket) and steel (PV clamp block) components, MQL produced the lowest cumulative exergy consumption compared with dry machining and flood cooling, reflecting reduced machining electricity demand, improved tool-life allocation, and lower rework/scrap penalties under the adopted dataset. These part-level reductions translate to lower embodied-exergy investment at the robotics-and-mounting kit level, strengthening lifecycle sustainability when combined with the operational benefit of robotics in maintaining PV yield under soiling conditions.

The study shows that credible sustainability evaluation of robotics-enabled green hydrogen mini-grids requires more than first-law efficiency reporting: second-law exergy analysis identifies where irreversibilities concentrate in operation, while manufacturing-stage CExC reveals how shop-floor decisions such as MQL adoption can reduce embodied thermodynamic burden and support lifecycle performance improvements. Future work should extend the presented demonstration to full-year, site-specific simulations using Nigeria irradiance and soiling data, validate robotics-induced PV yield factors in field deployments, and expand manufacturing inventories to include non-machining processes and supply-chain-specific exergy/emissions factors to strengthen local decision-making for green hydrogen mini-grids.

REFERENCES

[1] Nigerian Electricity Regulatory Commission (NERC), *Regulation for Mini-Grids 2016 (Regulation No: NER/-R-110/17)*, 2017.

[2] All On, *Simplified Guide to Nigeria's Mini-Grid Regulations*, 2017.

[3] H2Diplo (GIZ), "Nigeria launches National Hydrogen Policy Development to advance clean energy future," Feb. 21, 2025.

[4] "Investigating green hydrogen production operated by redundant energy on a solar PV mini-grid," *Int. J. Hydrogen Energy*, 2024, Art. no. S0360319924038084.

[5] A. Rosato, "Modelling the exergy of solar radiation: A review," *Energies*, vol. 15, no. 4, Art. no. 1477, 2022.

[6] EOLSS, "Exergy of Solar Radiation," sample chapter (PDF).

[7] I. Kishor, U. Mamodiya, V. Patil, and N. Naik, "AI-integrated autonomous robotics for solar panel cleaning and predictive maintenance using drone and ground-based systems," *Scientific Reports*, vol. 15, no. 1, 2025, doi: 10.1038/s41598-025-17313-6.

[8] Y. Wang and C. Liu, "State-of-the-art on minimum quantity lubrication in green machining," *J. Cleaner Prod.*, vol. 429, Art. no. 139613, 2023, doi: 10.1016/j.jclepro.2023.139613.

[9] ElectricityLawyer, *Simplified Legal and Regulatory Guide: Nigerian Electricity Regulatory Commission Mini-Grid Regulation* (noting updates aligned with the Electricity Act 2023), 2024.

[10] World Bank Group, "Global Solar Atlas—Nigeria (download and resource layers)," dataset page.

[11] EnergyData.info (World Bank/ESMAP), "Nigeria—Solar Radiation Measurement Data," dataset page.

[12] H. Chanchangi *et al.*, "Soiling mapping through optical losses for Nigeria," *Renewable Energy*, 2022, Art. no. S0960148122010151.

[13] "In-situ assessment of photovoltaic soiling mitigation techniques in northern Nigeria," Teesside University repository record.

[14] "Optimizing PV maintenance: Methods, cleaning frequency, and a selection framework," *MethodsX*, 2025, Art. no. S2352484725004238.

[15] "A comprehensive review on solar panel cleaning robot technologies," *AIP Conf. Proc.*, 2023.

[16] "AI-integrated autonomous robotics for solar panel cleaning and predictive maintenance…," *Scientific Reports*, 2025 (PDF).

[17] "Prototype optimization of autonomous solar cleaning robot," Springer journal article page, 2025.

[18] "A comprehensive review of direct coupled photovoltaic–electrolyser system: Sizing techniques, operating strategies, research progress, current challenges, and future recommendations," *Int. J. Hydrogen Energy*, 2023, Art. no. S0360319923013800.

[19] "Comparative analysis of PV-to-electrolyzer coupling configurations," Wiley (article/PDF page), 2024.

[20] "Modeling of photovoltaic–PEM hydrogen production system and coupling methods," 2024 (article page).

[21] "Solar-powered green hydrogen from electrolyzer systems: A review," Wiley (article/PDF page), 2025.

[22] "Energy/exergy/economic/carbon analyses of PV–PEM and related systems," *Int. J. Hydrogen Energy*, 2024.

[23] "Efficient solar-powered PEM electrolysis with battery assistance," Springer article page, 2024.

[24] UGent repository, "Exergy and cumulative exergy use analysis" (chapter/monograph record).

[25] "Electrochemical energy–exergy analysis of reversible solid oxide cell / storage-conversion devices," *J. Power Sources* (ScienceDirect article page), 2023.

[26] T. Gutowski, J. Dahmus, and A. Thiriez, "Electrical energy requirements for manufacturing processes," in *Proc. 13th CIRP Int. Conf. Life Cycle Engineering*, Leuven, Belgium, 2006.

[27] "State-of-the-art review of energy consumption in machining operations," *Renewable & Sustainable Energy Reviews*, 2025 (ScienceDirect journal/article entry).

[28] "Exergy loss assessment method for CNC milling system considering the energy consumption of the operator," *Processes* (MDPI), vol. 11, no. 9, Art. no. 2702, 2023.

[29] N. Liu *et al.*, "Progress and trend of minimum quantity lubrication (MQL): A comprehensive review," *J. Cleaner Prod.*, 2022/2023 (article page).

[30] "A comprehensive review of minimum quantity lubrication (MQL) machining technology," *Int. J. Adv. Manuf. Technol.*, 2024, doi: 10.1007/s00170-024-13902-3.

[31] "Recent advancements in minimum quantity lubrication (MQL)," *Lubricants* (MDPI), 2025 (article page).

[32] "A review of nanofluid minimum quantity lubrication (NFMQL) technology," *Lubricants* (MDPI), 2026 (article page).

[33] K. Maruthamuthu, K. Pandi, A. Sathasivam, and P. Palanisamy, "Recent advancements in machining processes using minimum quantity lubrication and nanofluids," *J. Tribol.*, vol. 147, no. 9, Art. no. 090801, Sep. 2025, doi: 10.1115/1.4069043.

[34] R. Peng *et al.*, "Performances of a tailored vegetable oil-based graphene nanofluid in the MQL internal cooling milling," *J. Manufacturing Processes*, 2024, Art. no. S1526612524013434.